Electronic Supplementary Material (ESI) for Materials Horizons.

Post-annealing of $MAPbI_3$ perovskite films with methylamine for efficient perovskite solar cells

Yan Jiang,[a] Emilio J. Juarez-Perez,[a] Qianqing Ge,[b] Shenghao Wang,[a] Matthew R. Leyden,[a] Luis K. Ono,[a] Sonia R. Raga,[a] Jinsong Hu,[b] Yabing Qi*[a]

[a]*Energy Materials and Surface Sciences Unit (EMSS), Okinawa Institute of Science and Technology Graduate University (OIST), 1919-1 Tancha Onna-son, Okinawa 904-0495 Japan*

[b]*CAS Key Laboratory of Molecular Nanostructure and Nanotechnology, Institute of Chemistry, Chinese Academy of Sciences (CAS), Beijing 100190, P.R. China*

*Corresponding author: Yabing.Qi@OIST.jp

Experimental section

Solar cell fabrication. FTO glass slides (7-8 Ω/□ , Opvtech.) were used as substrates and cleaned by sequentially sonicating in deionized water, ethanol, acetone, and isopropanol followed by UV-Ozone treatment for 15 min. For planar perovskite solar cells, an 80 nm TiO_2 compact (c-TiO_2) layer was deposited via spray pyrolysis at 480 °C from a precursor solution of titanium diisopropoxide bis(acetylacetonate) (75 wt% in isopropanol, Sigma-Aldrich) in 1-butanol (99.8%, Sigma-Aldrich) (m:m = 1.92:1). A 300 nm $MAPbI_3$ perovskite layer was spin-coated on the c-TiO_2 layer with 1:1 molar ratio of lead iodide (TCI, 99.99%) and methyl ammonium iodide (dyesol) in a mixed solution of DMSO (99.9%, Sigma-Aldrich) and DMF (99.8%, Sigma-Aldrich) (v:v = 1:11), using chlorobenzene (99.5%, Sigma-Aldrich) as the anti-solvent.[1] For methylamine solution exposure treatment, pre-annealed $MAPbI_3$ (100 °C for 10 min) was taped on the bottom of a beaker which was placed upside down. 200 μL of methylamine solution (33 wt. % in absolute ethanol, Sigma-Aldrich) was kept inside to maintain the atmosphere. MSE treatment finished after the film turned first transparent and then black again after exposure to air. For various post-annealing treatments, spin-coated precursor films were annealed on a hot plate of 100 °C for 10 min, covered with a glass petri dish to maintain the atmosphere. More specifically, 10 μL DMF, 20 μL methylamine solution or 20 μL ethanol were deposited on the petri dish for DMF solvent annealing, methylamine post-annealing or ethanol post-annealing, while no solvent was used for thermal annealing. A 200 nm hole transporting layer was spin-coated on the perovskite layer with a solution consisting of 72.3 mg spiro-MeOTAD (Merck), 28.8 μL of 4-*tert*-butyl pyridine and 17.5 μL of lithium bis(trifluoromethanesulfonyl)imide (Li-TFSI) solution (520 mg Li-TSFI in 1 mL acetonitrile (Sigma-Aldrich, 99.8 %)) in 1mL of chlorobenzene. Finally, an 80 nm Au electrode was

deposited via thermal evaporation at a constant rate of 0.03 nm/s. The fabrication of meso-structured perovskite solar cells was according to the literature with several changes.[2] In brief, 0.15 M titanium diisopropoxide dis(acetylacetonate) in 1-butanol was spin-coated on the FTO substrates, followed by drying at 125 °C for 5 min as the c-TiO_2 layer. A mesoporous TiO_2 layer was deposited on the c-TiO_2 by spin-coating the TiO_2 colloidal solution. After annealing at 550 °C in air, further treatment with 20 mM aqueous $TiCl_4$ (98%, Sigma-Aldrich) solution at 90 °C for 10 min was performed, followed by another annealing at 500 °C for 30 min. 500 nm $MAPbI_3$ perovskite was spin-coated on the mesoporous TiO_2 layer with the same precursor solution as before, but using diethyl ether as the anti-solvent. The same processes were employed for fabrication of the hole transporting layer and the Au electrode.

Film characterization. The morphology of perovskite films was characterized with field emission scanning electron microscopy (Helios NanoLab G3 UC, FEI) and atomic force microscopy (MFP-3D series, Asylum Research) in tapping-mode. The crystal structure was investigated with XRD (D8 Discover, Bruker). Absorbance was measured using a UV/Vis spectrometer (JASCO Inc., V-670). Surface chemical states were obtained from high resolution X-ray photoemission spectroscopy (Axis Ultra, KRATOS) with an Al Kα (1486.6 eV) X-ray source. The work function and the valence band edge were determined with ultraviolet photoemission spectroscopy (UPS) using a He I (21.2 eV) source. Chamber pressure was below 6.0E-9 Torr for XPS and UPS measurements. Time-resolved photoluminescence was acquired using the time-correlated, single-photon counting technique (Hamamatsu, C10627), and excitation was provided by a femtosecond mode-locked Ti:Sapp laser (Spectra-Physics, MAITAI XF-IMW) at 450 nm with an average power at 8 MHz of 0.74 mW.

Solar cell characterization. Photocurrent–voltage (J–V) characteristics and steady-state power output measurements were measured under AM 1.5 G one-sun illumination (100 mW/cm^2) using a solar simulator (Newport Oriel Sol 1A) and a Keithley 2400 source meter. Illumination intensity was calibrated with a monocrystalline silicon cell (Oriel Instruments Model Number 90026564). All measurements were performed with a 0.131 cm^2 mask calibrated by optical microscopy, in ambient air at 23–25 °C and a relative humidity of 50%, with 3s light pre-illumination. For J-V characteristics, scan rates were 0.2 V/s in both directions. For steady-state power output measurements, an algorithm was used that continuously adjusted the applied voltage to keep the power output of the device maximal. External quantum efficiency was measured using an Oriel IQE-200 measurement system in DC mode. Impedance spectra were obtained under 65.7 mW/cm^2 white illumination provided by a white LED lamp and using an FRA-equipped PGSTAT-204 potentiostat from Autolab. Impedance was recorded for various forward voltage biases over imposing an AC 20 mV voltage perturbation with the frequency ranging from 1 MHz to 10 mHz.

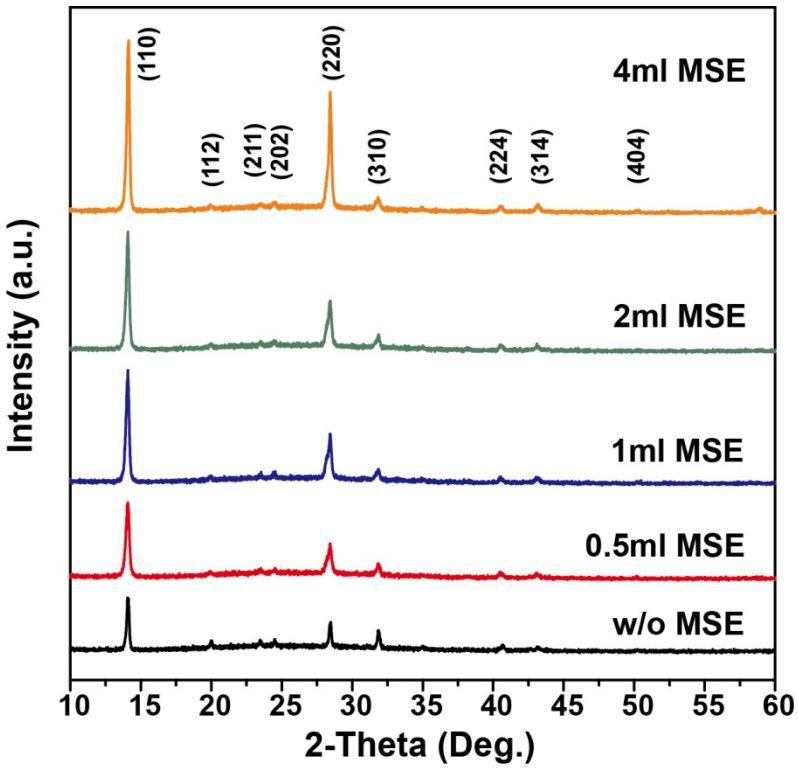

Fig. S1 XRD of perovskite films with various amount of methylamine solution during exposure. Increasing amounts of methylamine solution during exposure resulted in better perovskite crystallinity.

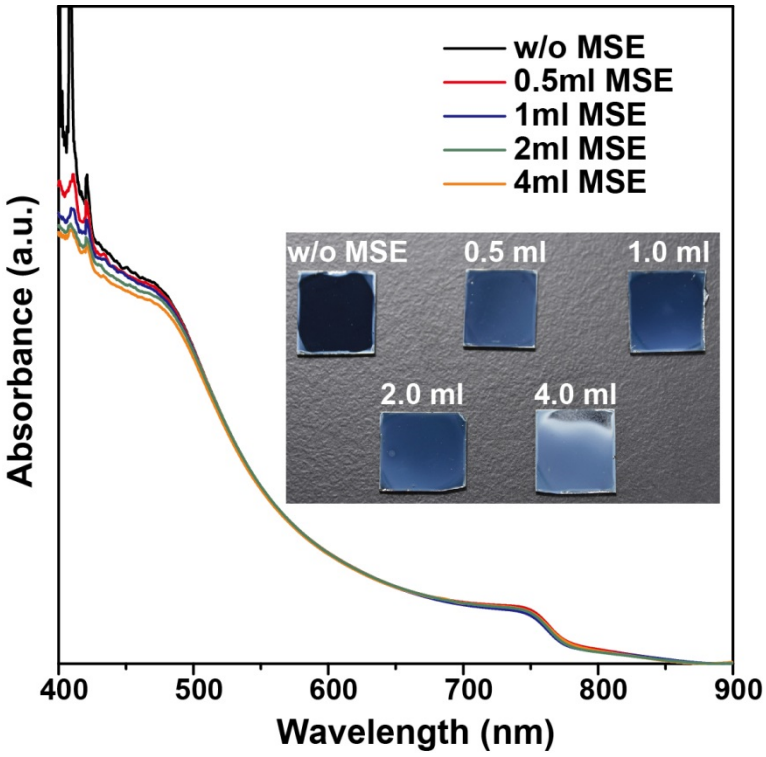

Fig. S2 UV-vis absorbance spectra of perovskite films with various amounts of methylamine solution during exposure. Photos of samples after different methylamine exposures are shown in the inset. With increasing amounts of methylamine solution during exposure, absorbance of perovskite films decreased, especially for photon wavelengths less than 500 nm. Uniformity of films also deteriorated.

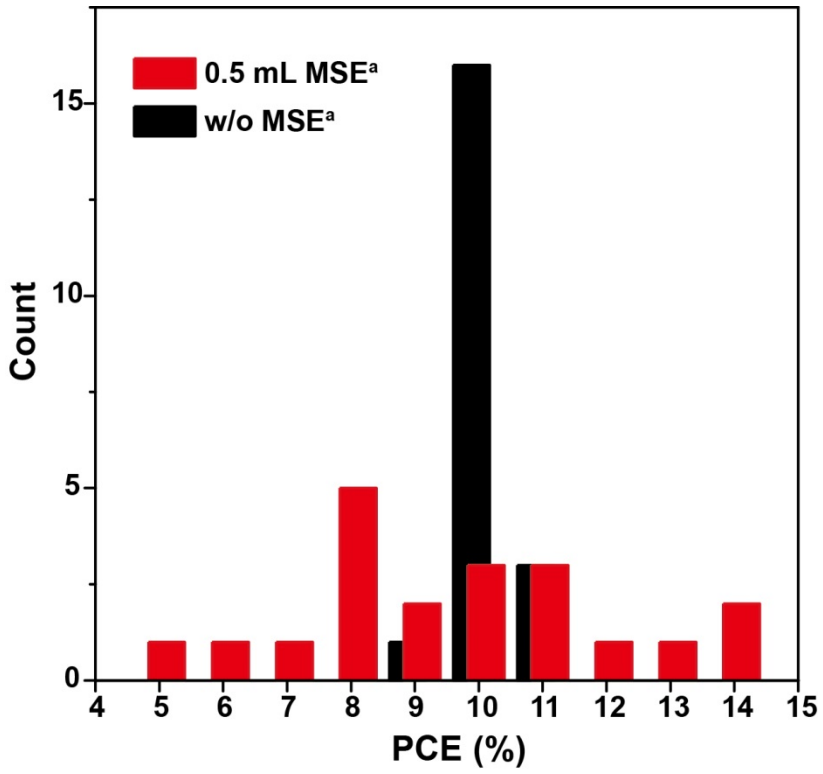

Fig. S3 Statistical analysis of power conversion efficiencies with and without methylamine solution during exposure. Superscript [a] represents the planar device. Planar perovskite solar cells subjected to MSE show large PCE variation compared to a batch of samples without MSE. No improvement can be inferred from comparisons of mean PCEs with and without MSE.

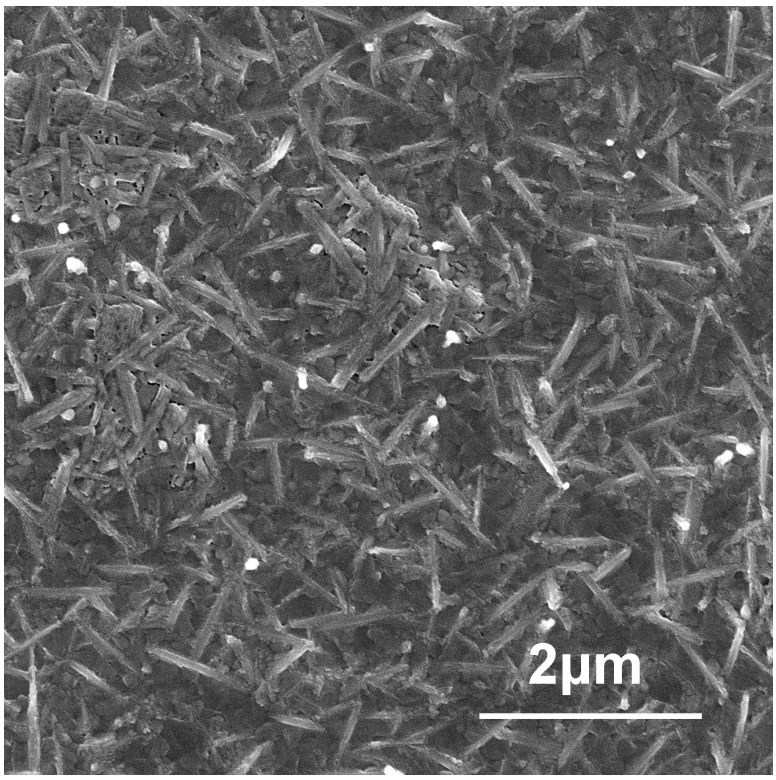

Fig. S4 SEM image of the pristine film without post-annealing treatment.

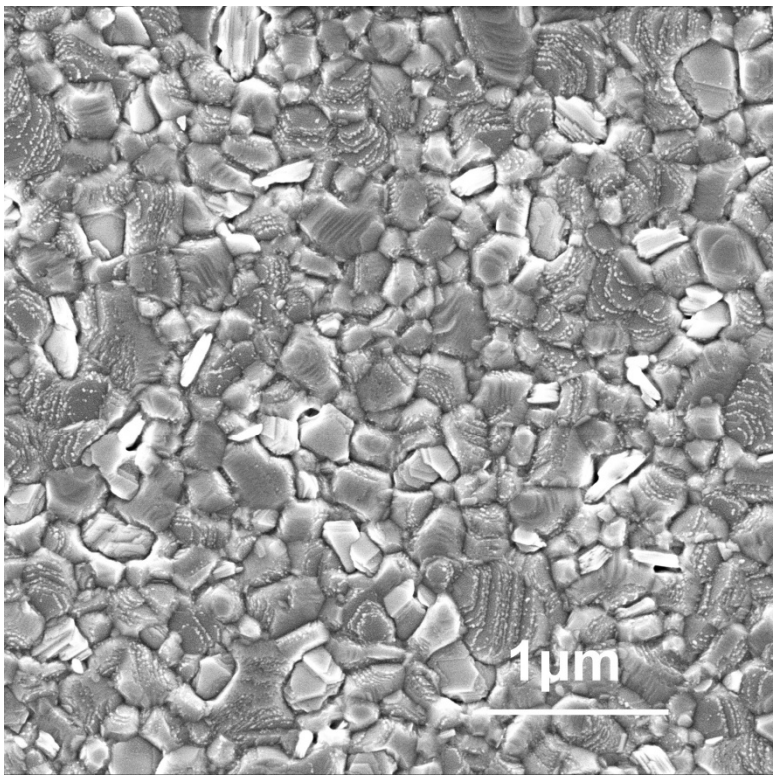

Fig. S5 SEM image of the $MAPbI_3$ perovskite film with ethanol post-annealing treatment. Perovskite films with thermal annealing (Fig. 2) and ethanol post-annealing show very similar surface morphology.

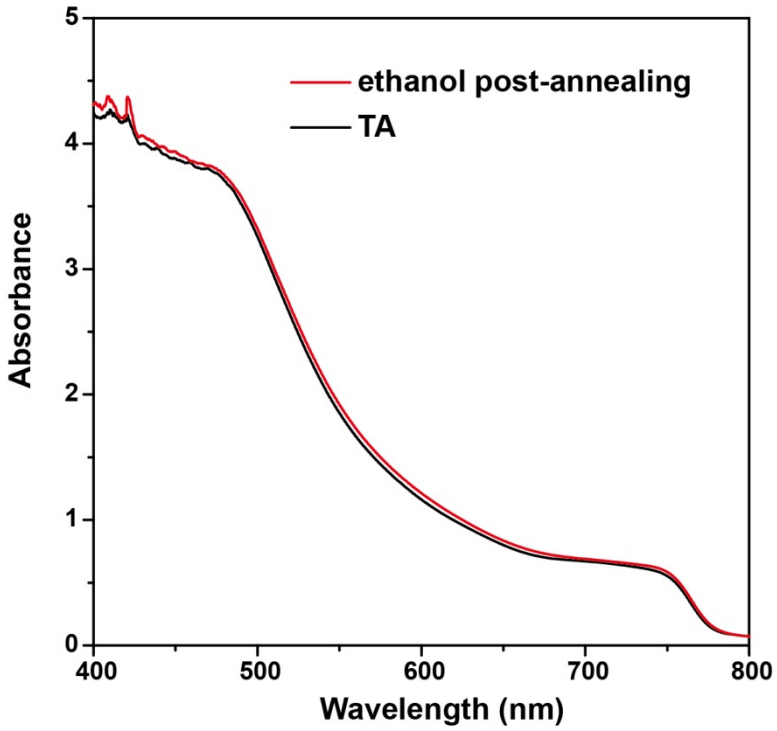

Fig. S6 UV-vis absorbance spectra of perovskite films with thermal and ethanol post-annealing. Perovskite films with these two different post-annealing treatments show similar absorbance edges and intensities.

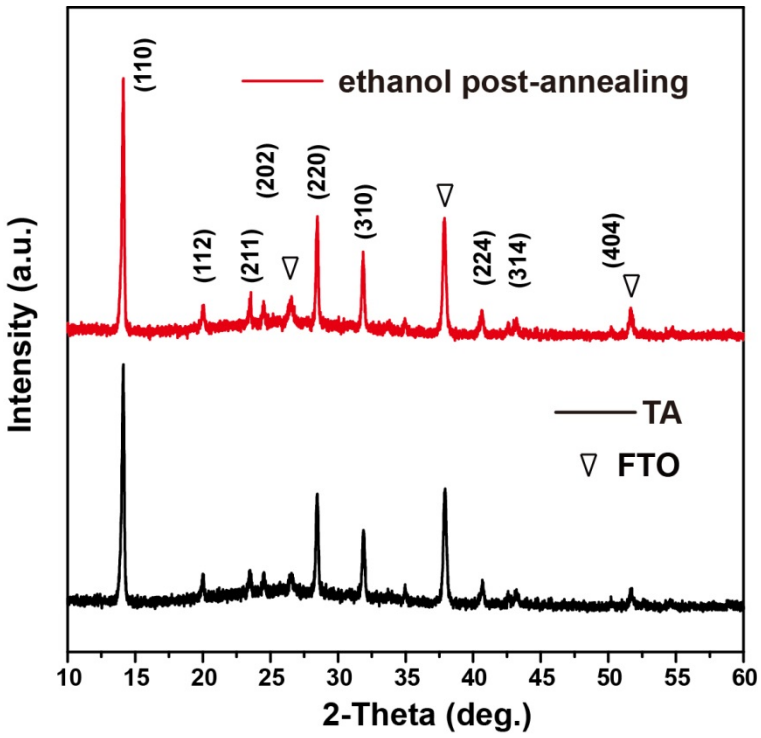

Fig. S7 XRD of perovskite films with thermal and ethanol post-annealing. Perovskite films with these two different post annealing treatments show similar peak positions and intensities.

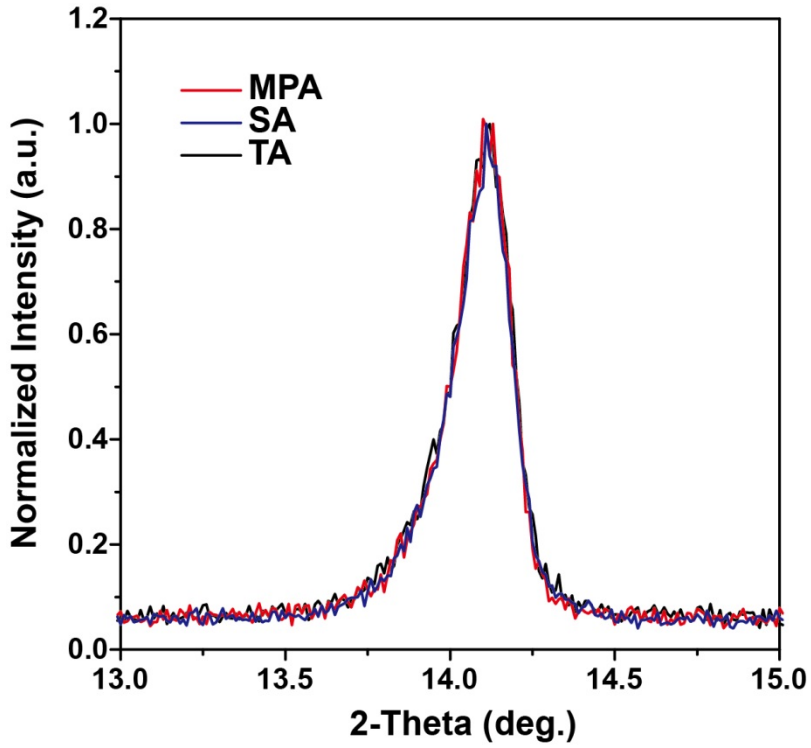

Fig. S8 XRD peak of $MAPbI_3$ perovskite (110) plane with TA, SA and MPA treatment. Perovskite films with various post-annealing treatments show similar crystallinity.

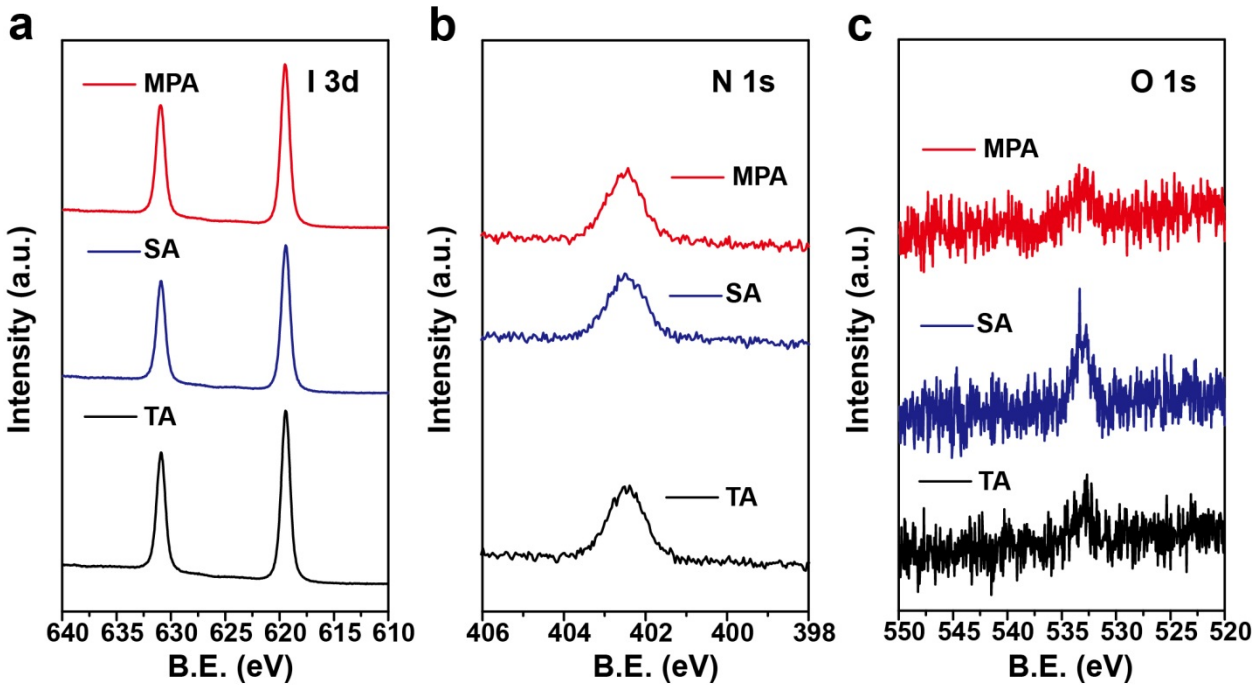

Fig. S9 HRXPS spectra of $MAPbI_3$ perovskite films with various post-annealing treatments. (a) I 3d, (b) N 1s and (c) O 1s core levels. MPA-treated films show fewer oxygen-related surface impurities than SA-treated films.

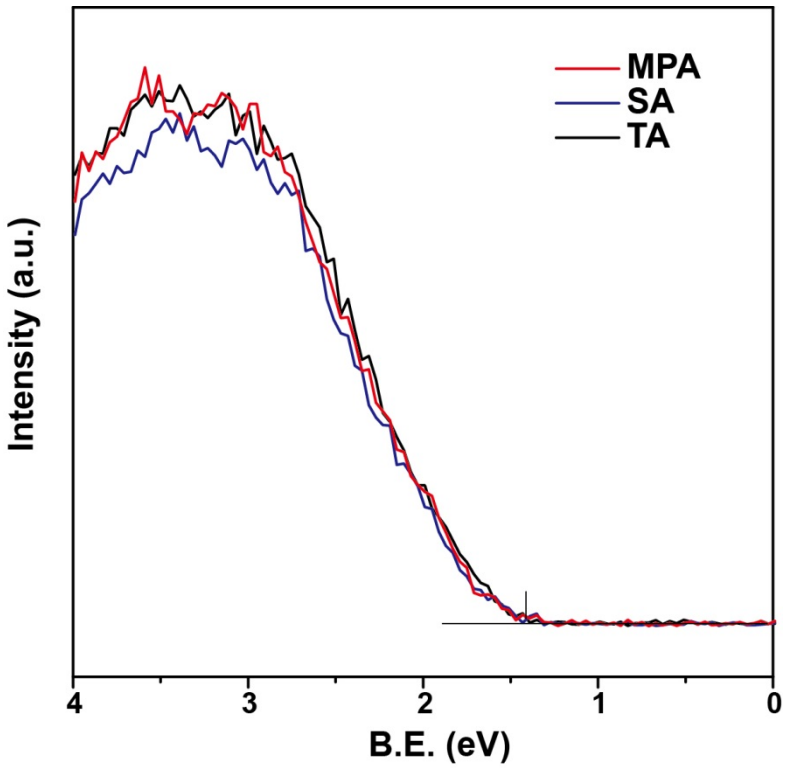

Fig. S10 Valence band region of XPS spectra of $MAPbI_3$ perovskite films with various post-annealing treatments. Perovskite films with various post-annealing treatments show similar valence band edges.

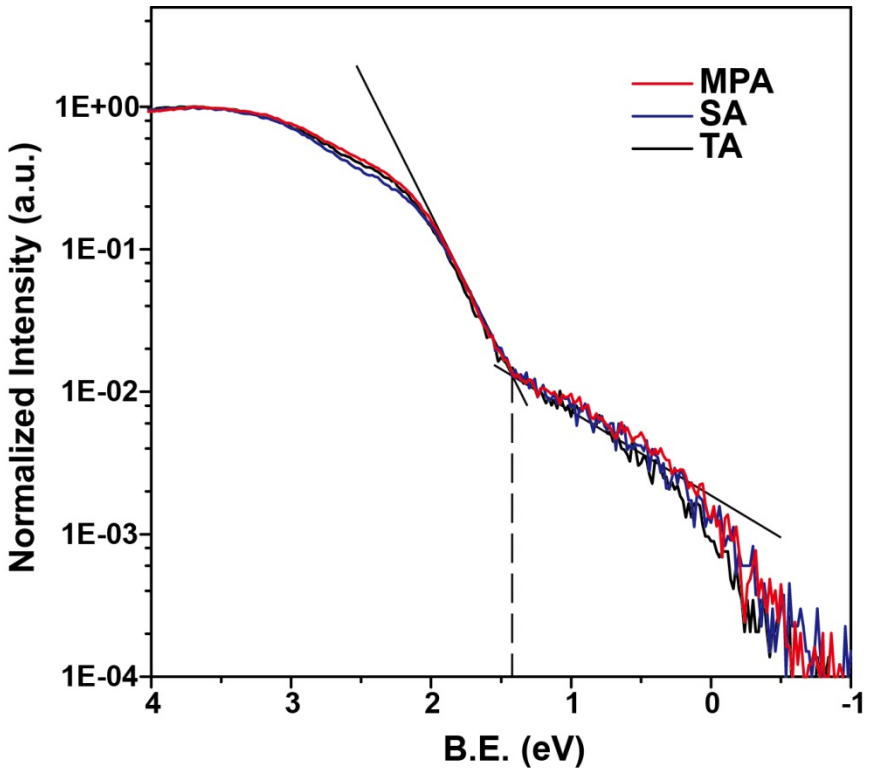

Fig. S11 Logarithmic scale of valence band region of UPS spectra of $MAPbI_3$ perovskite films with various post-annealing treatments. The valence band edges are located at 1.4 eV below the Fermi level for perovskite films with various post-annealing treatments.

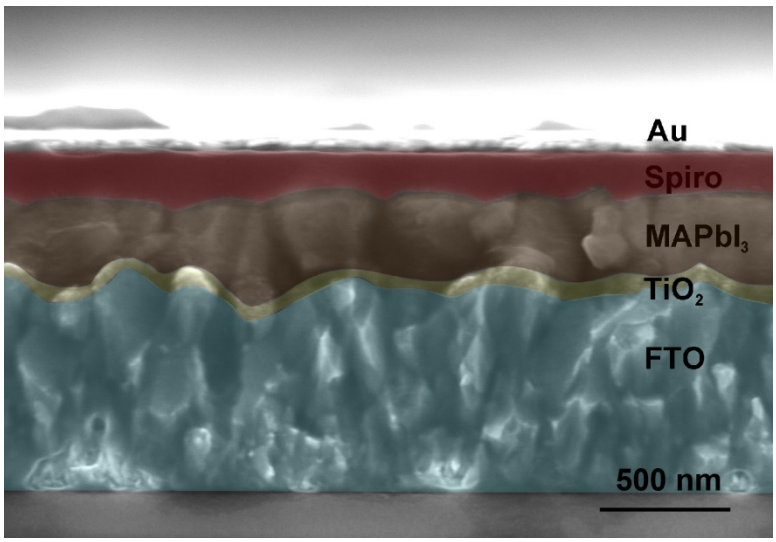

Fig. S12 Cross-sectional SEM image of the planar perovskite solar cell with MPA treatment.

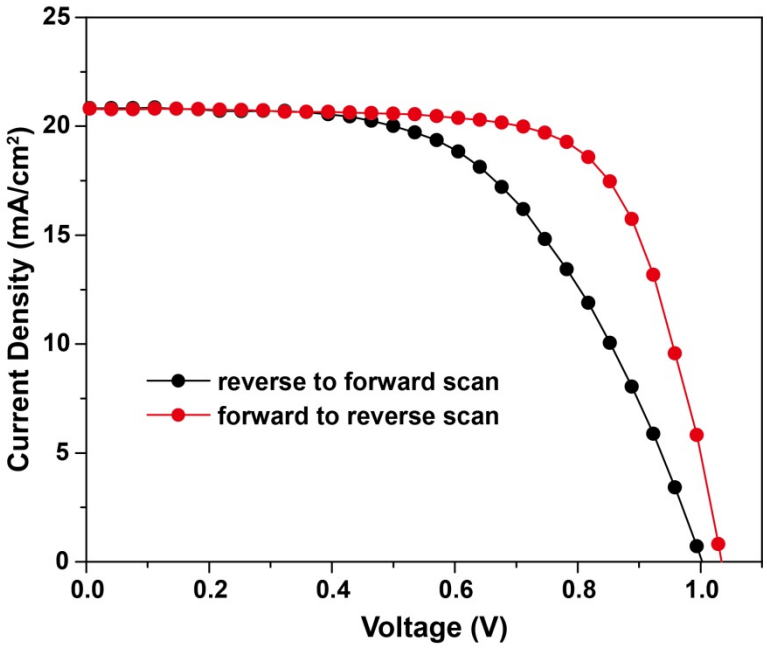

Fig. S13 Photocurrent−voltage (J−V) characteristics of the planar PSC with MPA treatment from different scan directions. A large mismatch in J-V curves exists between the two scan directions.

Table S1 Photovoltaic parameters of the perovskite solar cells with different scan directions.

	V_{oc} (V)	J_{sc} (mA/cm^2)	FF (%)	PCE (%)
Reverse to forward scan	1.00	20.8	54.0	11.4
Forward to reverse scan	1.03	20.8	70.6	15.2

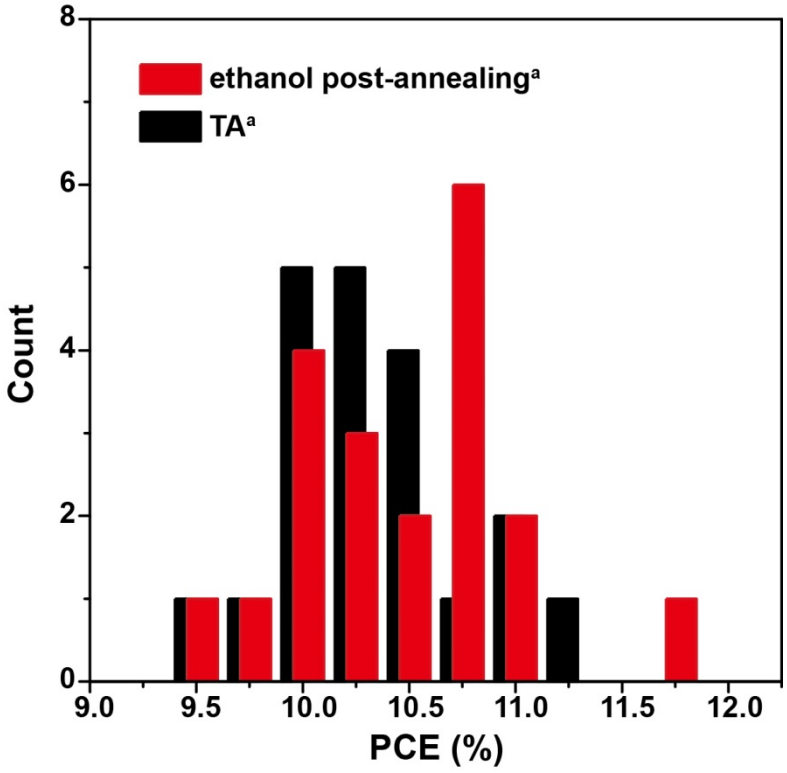

Fig. S14 Statistical analysis of power conversion efficiencies with thermal and ethanol post-annealing. [a] for planar devices. No significant improvement can be inferred from the ethanol post annealing.

Table S2 Photovoltaic parameters of the planar PSCs with thermal and ethanol post-annealing.

	V_{oc} (V)	J_{sc} (mA/cm^2)	FF (%)	PCE (%)
Thermal annealing[a]	1.00±0.02 (1.00)	19.6±0.4 (19.5)	53.5±2.9 (58.5)	10.5±0.4 (11.4)
Ethanol post-annealing[a]	1.00±0.03 (1.03)	20.0±0.4 (20.5)	53.1±2.1 (57.2)	10.6±0.5 (11.9)

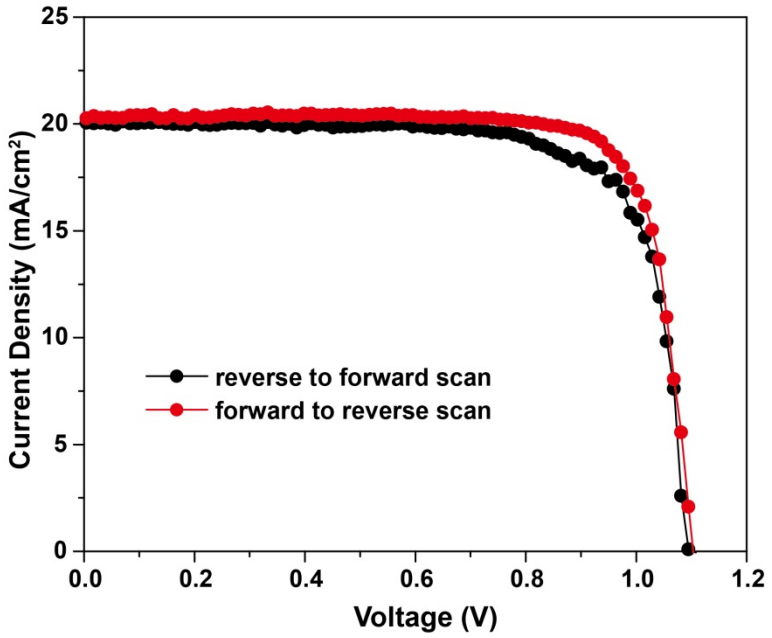

Fig. S15 Photocurrent−voltage (J−V) characteristics of the meso-structured PSC with MPA treatment from different scan directions. Hysteresis from different scan directions is significantly reduced compared with planar PSC.

Table S3 Photovoltaic parameters of the perovskite solar cells with different scan directions.

	V_{oc} (V)	J_{sc} (mA/cm^2)	FF (%)	PCE (%)
Reverse to forward scan	1.10	20.2	74.3	16.7
Forward to reverse scan	1.10	20.3	80.0	17.9

Reference

1. M. Xiao, F. Huang, W. Huang, Y. Dkhissi, Y. Zhu, J. Etheridge, A. Gray-Weale, U. Bach, Y. Cheng, L. Spiccia, *Angew. Chem. Int. Ed.,* 2014, **53**, 9898-9903.

2. N. Ahn, D. Y. Son, I. H. Jang, S. M. Kang, M. Choi, N. G. Park, *J. Am. Chem. Soc.,* 2015, **137**, 8696-8699.